High-Resolution Microscopy

DOI: 10.1002/anie.200906752

Imaging MoS_2 Nanocatalysts with Single-Atom Sensitivity**

*Christian Kisielowski, Quentin M. Ramasse, Lars P. Hansen, Michael Brorson, Anna Carlsson, Alfons M. Molenbroek, Henrik Topsøe, and Stig Helveg**

Materials derived from layered dichalcogenides, such as MoS_2, are of wide nanotechnological interest,[1] for instance as nanocatalysts for industrial oil refinement, hydrogen evolution, and photooxidation.[2–4] The MoS_2 structure basically consists of two-dimensional S–Mo–S slabs (Figure 1 a), which are stacked to various degrees.[5] However, direct information on the atomic-scale structure of MoS_2 nanocatalysts that are used in industry can be difficult to obtain. Information was previously obtained from scanning tunneling microscopy of model catalysts prepared under ultra-high vacuum conditions on planar, single-crystalline supports, and from density functional theory calculations.[6] The information from the model studies is difficult to relate to technologically relevant catalysts because the morphology and distribution of the catalytically important edge sites of the MoS_2 slabs are found to be sensitive to the preparation conditions, edge-attached promoter atoms, and interactions with support media.[7–9] For a long time, a key goal has therefore been to obtain high-resolution microscopy images on industrial-style MoS_2 nanocatalyst systems. Although high-resolution microscopy provides a powerful means for imaging industrial catalysts at different length scales,[10–12] atomically resolved images of the supported MoS_2 slabs in a (001) projection have not been available because of insufficient image contrast or resolution.[13–14] Recently advances in high-resolution transmission electron microscopy (HRTEM) have made it possible to obtain images of unsupported one-atom-thick films with single-atom sensitivity.[15] Herein, we report how the imaging technique was applied to obtain atomically resolved information on the shape and structure of MoS_2 nanocatalysts prepared in an industrial style.

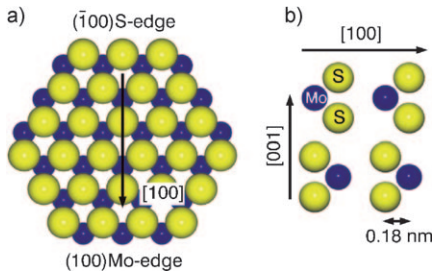

Figure 1. a) Ball model of a single-layer MoS_2 nanocrystal viewed along the (001) projection. The hexagonally arranged Mo atoms (blue balls) are trigonal prismatically coordinated to S atoms (yellow balls) in two adjacent layers. The bulk-truncated nanocrystal exposes a Mo- and S-edge termination. b) The 2H stacking sequence of two successive, single-layer MoS_2 slabs viewed along the ⟨110⟩ direction. The Mo planes are separated by 0.615 nm along the [001] direction and are translated and rotated so the in-plane positions of the S atoms in one layer coincide with the positions of the Mo atoms in the other layer and vice versa. The projected distance between neighboring Mo and S columns in a single layer along the ⟨100⟩ direction is 0.18 nm.

The nanocatalysts were synthesized on a graphitic carbon powder by the same methods used for the manufacture of industrial catalysts for oil-refinery hydrotreatment processes.[14] Details on the sample preparation and electron microscopy are provided in the Supporting Information. Figure 2 shows the experimentally restored phase of a complex exit wave function of the catalyst, and reveals a nanometer-sized particle situated on a thin graphite flake. The wave reconstruction was performed to recover all obtainable information contained in a series of 15 HRTEM images of the nanoparticle acquired at different focal points.[12] In such a phase image, the intensity maxima relate to atom positions and the contrast can reflect the chemical composition as represented in the projected scattering potential. Whilst the hexagonal shape of the nanoparticle is consistent with previously obtained images of this material,[14] the regular lattice in the interior part of the particle is now clearly visible. A lattice fringe pattern, which arises from the graphite lattice, is also seen on the surrounding support. A Fourier transform analysis of the image (Figure 2 a) reveals lattice spacings corresponding to the MoS_2 (100) and (110) as well as the graphite (100) lattice planes. Hence the nanoparticle reflects a MoS_2 nanocrystal oriented with its (001) basal plane parallel to the graphite support and orthogonal to the electron beam, consistent with model MoS_2 nanocatalysts on highly oriented pyrolytic graphite.[16] The contrast changes slightly over the projected area of the nanocrystal (Figure 2 a), which is likely due to the fact that even a slight localized bending of the

[*] Dr. C. Kisielowski, Dr. Q. M. Ramasse
National Center for Electron Microscopy
Lawrence Berkeley National Laboratory
1 Cyclotron Road, Berkeley, CA 94708 (USA)
Dr. A. Carlsson
FEI Company
Achtseweg Noord 5, 5651 GG Eindhoven (The Netherlands)
Dr. L. P. Hansen, Dr. M. Brorson, Dr. A. M. Molenbroek, Dr. H. Topsøe, Dr. S. Helveg
Haldor Topsøe A/S
Nymøllevej 55, 2800 Kgs. Lyngby (Denmark)
E-mail: sth@topsoe.dk

[**] Microscopy was performed at NCEM, which is supported by the Office of Science, Office of Basic Energy Sciences of the U.S. Department of Energy under contract no. DE-AC02-05CH11231. The research was carried out for the Helios Solar Energy Research Center, which is funded under contract no. DE-AC02-05CH11231.

Supporting information for this article is available on the WWW under http://dx.doi.org/10.1002/anie.200906752.

WILEY InterScience DISCOVER SOMETHING GREAT

© 2010 Wiley-VCH Verlag GmbH & Co. KGaA, Weinheim

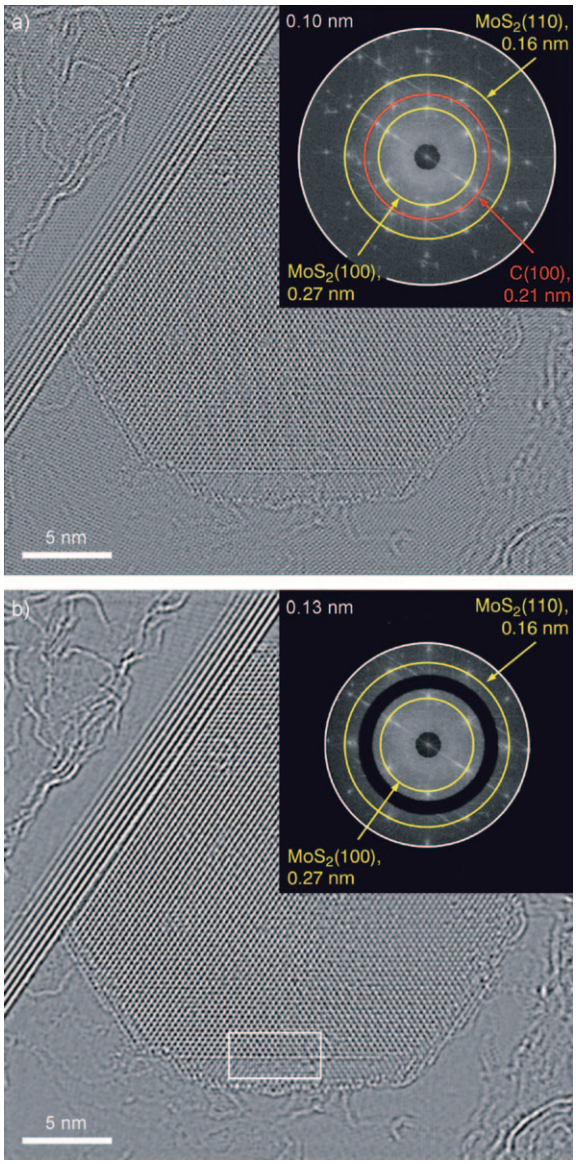

Figure 2. a) Reconstructed phase of the aberration-corrected exit wave function of a MoS_2 nanocrystal supported on graphite recorded along the MoS_2 ⟨001⟩ direction. The inset shows a fast Fourier transform of this image and shows clearly the distinct 0.27 nm and 0.16 nm lattice distances, which correspond to the MoS_2 (100) and (110) lattice planes, respectively. The 0.21 nm lattice distance, which corresponds to the graphite (100) lattice planes, is also shown. The outer ring at 0.10 nm corresponds to the instrument information transfer limit. b) The graphite support contribution to the reconstructed phase was filtered with a frequency domain filter ranging from 4.4 to 5.2 nm^{-1} and beyond 7.7 nm^{-1}. The outer ring at 0.13 nm corresponds to the limit of flat information transfer and indicates the spatial resolution of the phase restoration. A white box indicates the region used for quantitative analysis.

nanocrystal may result in a detectable, albeit minute, defocus change in state-of-the-art instruments. As the phase image represents a projection of both the nanocrystal and its support, the information from the graphite lattice can be filtered out in reciprocal space (Figure 2b) to reveal the information that pertains solely to the MoS_2 nanocrystal.

At the atomic level, two distinct and uniform contrast patches can be seen near the bottom edge of the MoS_2 nanocrystal and are clearly recognized on the colored close-up of the region (Figure 3). To provide a quantitative measure

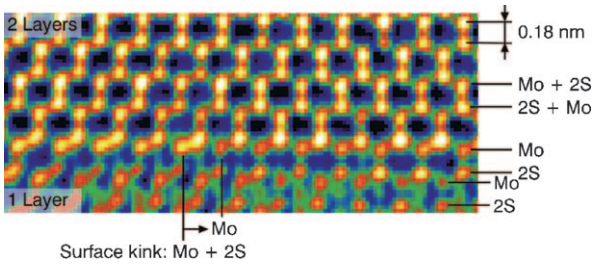

Figure 3. A close-up of the phase image obtained from the region near the bottom edge of the MoS_2 nanocrystal (partly contained in the white box of Figure 2b). A red-green-blue color scale was applied to improve readability. The upper region is assigned to a double-layer MoS_2 slab, while the lower region is a single-layer slab. More generally, the chemical composition of individual columns can unambiguously be determined. A kink from a Mo + 2S column to a Mo column is indicated along the surface step from the double-layer to the single-layer MoS_2.

of the signal and noise in the upper (brighter) and lower (darker) patches (Figure 4a), averages were obtained by template-matching across the selected region (white box in Figure 2b). Linescans taken along the [100] direction in the resulting averaged patches clearly reveal an intensity pattern containing two maxima separated by 0.18 nm (Figure 4b), corresponding to the separation between the atomic columns of MoS_2 in the (001) projection. Whilst the intensity level of all maxima is the same in the upper patch, a statistically significant variation between neighboring columns is observed in the lower patch. Furthermore, the average intensity of the upper patch is roughly twice that of the lower patch. These contrast variations in the experimental phase therefore suggest that the upper region corresponds to a double-layer slab, where each column contains one Mo atom and two S atoms in a 2H stacking sequence of MoS_2 layers (i.e., Mo + 2S or 2S + Mo columns; Figure 1b), whereas the lower region corresponds to a single-layer slab where alternating columns contain one Mo atom or two S atoms (i.e., Mo or 2S columns). To confirm this interpretation, detailed simulations of the exit wave function are presented (Figure 4b). The simulated phase for a double-layer MoS_2 slab exhibits peaks with the same intensity and a separation of 0.18 nm along the [100] direction; this simulation is in good agreement with the experimentally reconstructed phase. In turn, the simulated phase for the 2S column of a single-layer MoS_2 slab presents a peak with higher intensity than its neighboring Mo column, with intensity levels that again match the experimental results. The excellent agreement between simulation and experiment thus provides unprecedented chemical identification of the atomic columns of the nanocatalyst by simply matching the phase intensity levels. A surface step along the ⟨110⟩ direction from the double-layer slab to the single-layer slab, including an apparent kink site, can thus be readily identified (Figure 3). The present analysis

 © 2010 Wiley-VCH Verlag GmbH & Co. KGaA, Weinheim

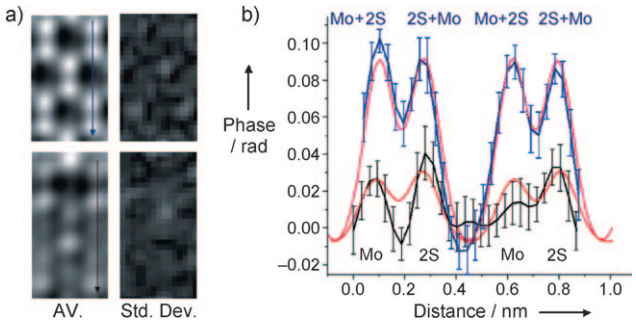

Figure 4. a) Template-averaged patches (left) and standard deviations (right) obtained from the double-layer (upper displays) and single-layer (lower displays) regions in the area indicated in Figure 2b. b) Line-scans along the [100] direction reveal a double intensity profile with varying intensity levels, which match multislice exit wave function simulations. In a single layer, the contrast from one Mo atom differs significantly from the contrast of two S atoms, thus allowing for element identification. The experimental error bars correspond to two standard deviations from the average. Scans show experimental (black line = single layer; blue line = double layer) and simulated (red line = single layer; pink line = double layer) results.

focuses entirely on the bulk area of the nanocrystal that remained stationary during imaging. At the very edge of the single layer (just below the box of Figure 2b), a slightly brighter and blurred contrast resulted from edge atom restructuring between consecutive images of the present focal series.

The observed element pattern in the basal plane (Figure 3) allows an unambiguous assignment of the single-layer edge termination as that of a Mo edge (see Figure 1a). In this context, the clear distinction between single- and double-layer slabs, as well as the direct observation of the 2H stacking of the double-layer slab, is also important, because the 2H sequence implies that the successive MoS_2 layers will expose alternating Mo- and S-edges and hence an equal concentration of the different edge types, independent of the double-layer shape (see Figure 1b). The element-sensitive imaging of MoS_2 nanocatalysts thus allows the type and the concentration of the catalytically important edge sites to be estimated, which was not previously possible for industrial-style MoS_2 nanocatalysts. In the future, it will therefore be possible to combine the structural information with reactivity data and establish site-specific catalytic information. Hence, this approach opens up possibilities for improving the formulation of the MoS_2 nanocatalyst properties. The ability to image the detailed atomic arrangement of nanocatalysts with a sensitivity at the single-atom level should be generally applicable and should help to establish new relationships between the atomic structure and functionality of technological relevant nanocatalysts.

Received: November 30, 2009
Published online: March 15, 2010

Keywords: chalcogens · electron microscopy · heterogeneous catalysis · molybdenum · single-atom imaging

[1] R. Tenne, *Angew. Chem.* **2003**, *115*, 5280 – 5289; *Angew. Chem. Int. Ed.* **2003**, *42*, 5124 – 5132; R. Tenne, *Nat. Nanotechnol.* **2006**, *1*, 103 – 111.
[2] R. Prins, *Adv. Catal.* **2001**, *46*, 399 – 464.
[3] B. Hinnemann, P. G. Moses, J. Bonde, K. P. Jørgensen, J. H. Nielsen, S. Horch, I. Chorkendorff, J. K. Nørskov, *J. Am. Chem. Soc.* **2005**, *127*, 5308 – 5309.
[4] J. P. Wilcoxon, T. R. Thurston, J. E. Martin, *Nanostruct. Mater.* **1999**, *12*, 993 – 997.
[5] a) K. P. de Jong, L. C. A. van den Oetelaar, E. T. C. Vogt, S. Eijsbouts, A. J. Koster, H. Friedrich, P. E. de Jongh, *J. Phys. Chem. B* **2006**, *110*, 10209 – 10212; b) E. J. M. Hensen, P. J. Kooymann, Y. van der Meer, A. M. van der Kraan, V. H. J. de Beer, J. A. R. van Veen, R. A. van Santen, *J. Catal.* **2001**, *199*, 224 – 235.
[6] F. Besenbacher, M. Brorson, B. S. Clausen, S. Helveg, B. Hinnemann, J. Kibsgaard, J. V. Lauritsen, P. G. Moses, J. K. Nørskov, H. Topsøe, *Catal. Today* **2008**, *130*, 86 – 96.
[7] H. Schweiger, P. Raybaud, G. Kresse, H. Toulhoat, *J. Catal.* **2002**, *207*, 76 – 87.
[8] J. V. Lauritsen, S. Helveg, E. Lægsgaard, I. Stensgaard, B. S. Clausen, H. Topsøe, F. Besenbacher, *J. Catal.* **2001**, *197*, 1 – 5.
[9] B. Hinnemann, J. K. Nørskov, H. Topsøe, *J. Phys. Chem. C* **2005**, *109*, 2245 – 2253.
[10] a) B. M. Weckhuysen, *Angew. Chem.* **2009**, *121*, 5008 – 5043; *Angew. Chem. Int. Ed.* **2009**, *48*, 4910 – 4943; b) E. de Smit, et al., *Nature* **2008**, *456*, 222 – 226; see Supporting Information.
[11] A. K. Datye, *J. Catal.* **2003**, *216*, 144 – 154.
[12] L. C. Gontard, L.-Y. Chang, C. J. D. Hetherington, A. I. Kirkland, D. Ozkaya, R. E. Dunin-Borkowski, *Angew. Chem.* **2007**, *119*, 3757 – 3759; *Angew. Chem. Int. Ed.* **2007**, *46*, 3683 – 3685.
[13] R. M. Stockmann, H. W. Zandbergen, A. D. van Langeveld, J. A. Moulijn, *J. Mol. Catal. A* **1995**, *102*, 147 – 161.
[14] M. Brorson, A. Carlsson, H. Topsøe, *Catal. Today* **2007**, *123*, 31 – 36.
[15] a) N. Alem, R. Erni, C. Kisielowski, M. D. Rossell, W. Gannett, A. Zettl, *Phys. Rev. B* **2009**, *80*, 155425; b) C. Girit, et al., *Science* **2009**, *323*, 1705 – 1708; see Supporting Information.
[16] J. Kibsgaard, J. V. Lauritsen, E. Lægsgaard, B. S. Clausen, H. Topsøe, F. Besenbacher, *J. Am. Chem. Soc.* **2006**, *128*, 13950 – 13958.

 © 2010 Wiley-VCH Verlag GmbH & Co. KGaA, Weinheim